Thermo-flow behavior of air-channel heat exchanger with nonidentical baffle lengths: computational analysis

Anas Alwatban[1] · Ahmad Aljabr[2]

Abstract

Previous research assumed the same baffle size across a heat exchanger with two baffles although the flow characteristics change along the channel. This present work suggests a novel design of using nonidentical baffle lengths along the channel because the best baffle length is not the same for both baffles. The main objective of this suggested design is to enhance the thermal enhancement factor (TEF) of a regular heat exchanger with baffles. After studying 16 cases of different baffle sizes using a two-dimensional channel in ANSYS Fluent software, it is found that the baffles with the same length do not always achieve the best TEF. When the second baffle is half the length of the first baffle, TEF increases by 3%, and the upper wall friction factor decreases by about 50%. In addition, it is found that the average Nusselt number of the upper wall is sensitive to the length of both baffles. From these results, the assumption that the baffles inside the channel should not be identical in length is authentic.

Abbreviations

TEF	Thermal enhancement factor
TKE	Turbulence kinetic energy

List of symbols

C_p	Specific heat (J kg^{-1} K^{-1})
C_f	Skin friction coefficient
D_h	Hydraulic diameter (m)
f	Friction factor
H	Heat exchanger height (m)
h	Heat transfer coefficient (W m^{-2} K^{-1})
k	Turbulent kinetic energy
k_f	Fluid thermal conductivity (W m^{-1} K^{-1})
L	Heat exchanger length (m)
Nu	Nusselt number
P	Static pressure (*Pa*)
P_d	Dynamic pressure (*Pa*)
Pr	Prandtl number
Re	Reynolds number
T	Temperature (K)
u	Fluid velocity in x-direction (m s^{-1})
v	Fluid velocity in y-direction (m s^{-1})
W	Heat exchanger width (m)

Greek symbols

ε	Turbulent rate of dissipation
μ_l	Dynamic viscosity (N s m^{-2})
μ_t	Turbulent viscosity (N s m^{-2})
ρ	Density (kg m^{-3})

✉ Ahmad Aljabr
aa.aljabr@mu.edu.sa

1 Department of Mechanical Engineering, College of Engineering, Qassim University, 51452 Buraydah, Qassim, Saudi Arabia

2 Department of Mechanical and Industrial Engineering, College of Engineering, Majmaah University, Majmaah 11952, Saudi Arabia

Introduction and background

Heat exchangers are widely used to transfer heat between two fluids. They come in different types and sizes based on the required function. The heat transfer rate can be enhanced by different ways such as using various designs [1], adding fins or baffles [2, 3], using specific flow arrangement [4, 5], or using nanofluids [6–8]. The heat exchanger is designed so the fluid has turbulent flow to increase the heat transfer rate between the two fluids. One way to generate turbulence is by adding baffles at different locations though the channel which disturb the direction of the flow and create recirculating flows and boundary layer separation. There are numerous applications that could benefit from using heat exchanger

with baffles such as solar air heater, shell–tube heat exchangers, and electronic devices coolers. However, enhancing the heat transfer rate by generating turbulence with baffles comes at the expense of increasing the pressure drop, which means increasing the pumping power requirement.

There have been many studies that, experimentally and numerically, examined the effect of different various characteristics of the baffles such as their length, shape, depth, inclination, material, and distance [9]. The pressure drop, the heat transfer rate, the temperature change, and the velocity profile are some of the properties that are under examined when the baffle characteristics are changed in those studies.

One way to examine the enhancement in the heat transfer rate with utilizing baffles is by using different shapes of baffles. Brahimi et al. [10] studied the 2D velocity, pressure, and temperature fields at different shapes of baffles (square, trapezoidal, and three types of triangular shapes) using ANSYS software. Cao et al. [11] presented a sextant helical baffle to overcome the leakage in the regular helical baffles. Their suggested model was studied experimentally, and a numerical model was used for detailed scrutiny in terms of the heat transfer coefficient, pressure drop, and friction factor. They found that the sextant helical baffle has better performance in terms of the heat transfer coefficient and pressure drop. Another baffle shape was introduced by Skullong et al. [12] to study the heat transfer rate and the friction factor inside a squared duct. The baffle has a horseshoe shape which was examined at three baffle pitches and five baffle heights at various values of Reynolds number. Promvonge et al. [13] investigated a flapped V-shaped baffle inside a solar receiver channel at four flap angles, three baffle pitches, and one baffle height and length. The flapped V-shaped was found to achieve 2.5 times the thermal performance. The Nusselt number and the friction factor were the main parameters in this study. Another baffle shape is a diamond shape which was studied by Saha [14] and compared with regular rectangular baffle in terms of the velocity profile, friction factor, and Nusselt number. Additional extensive study by Menni et al. [15] examined V-shaped baffles at various attack angles, lengths, and distances at different Reynolds number values. The results showed that the thermal enhancement factor has an optimum value at attack angle of 40° at highest flow rate and fin length of 0.08 m. Also, the heat transfer rate increased with increasing the distance between the baffles but with an increase in the friction factor. Increasing the baffle length or reducing the distance between them showed a growth of the recirculation of fluid. T-shaped baffles were investigated by Medjahed et al. [16] at different Reynolds numbers. The thermal transfer rate was enhanced at high flow rate due to the increase in the fluid recirculation and the negative turbulence kinetic energy around the baffles. The authors claimed that the suggested model improved the thermal enhancement factor by 2–26% compared to other shapes of baffles in the literature.

The size and tilt of the baffles have been other ways to examine the enhancement in the heat transfer rate with minimizing the drop in fluid pressure. Mohammadi et al. [17] evaluated the performance of a single-pass solar air heater at different sizes of the fins and baffles in a steady-state case. Although the fins and baffles enhanced the efficiency and outlet air temperature, higher size of fins and baffles could reduce the efficiency of the system due to the increase in the required pumping power. The authors found that the optimum number of fins and baffles is case-specific depending on the constant mass flow rate. Also, the baffle width was found to be significant at high value of Reynolds number (turbulent flow). Kumar et al. [18] also evaluated the performance of a triangular duct solar air heater with rectangular ribs using ANSYS Fluent software. The friction factor, Nusselt number, roughness height, and roughness pitch were examined under various values of Reynolds number and rib aspect ratio, and optimum thermohydraulic performance was obtained. El-Said et al. [19] conducted an experiment to test four kinds of baffle configurations (conventional single segmental baffle, staggered single segmental baffle, flower segmental baffle, and hybrid segmental baffle). The results showed that the last four configurations enhanced the heat transfer rate. Although the hybrid segmental baffle has the highest heat transfer rate, it resulted in the highest flow resistance. Marzouk et al. [20] studied those same four kinds of baffle configurations (in El-Said et al. [19]) in addition to circular ring baffle and circular ring baffles with holes. At various values of Reynolds number, the heat transfer rate, pressure drop, and effectiveness were examined. They found out that different baffle configurations have a significant impact on the pressure drop and heat transfer coefficient. El Habet et al. [21] examined the effect of the tilting angle of staggered baffles on the heat transfer parameters in a rectangular channel at a range of Reynolds number. It was found that the small tilt angle has the highest heat transfer enhancement and lowest friction factor, while the large tilt angle has the lowest heat transfer enhancement and largest friction factor. Also, stronger recirculation and reattachment flow was obtained at low tilting angles and low perforation ratios. The optimum thermal enhancement factor was found at the largest tilt angles and minimum perforation ratio at specific Reynolds number. Rebhi et al. [22] investigated the effect of staggered rectangular baffles with square fins in between at various shapes, fixations, and arrangements using k-ε turbulence model. The authors described only the temperature, velocity, and pressure fields. The baffle in the head of heat exchanger was examined by Kitayama et al. [23] to optimize the diameter of holes in the baffles. The objective functions that must be minimized were the pressure drop and the flow nonuniformity. The optimized result showed

that the pressure drop and the flow nonuniformity have been minimized as well as the large vortex size.

Another technique to enhance the heat transfer rate by using baffles with minimum pressure drop is the use of metal foam in baffles instead of solid baffles. Fadhala et al. [24] used a copper foam baffles with a gradient pore density to override the low heat transfer efficiency of regular metal foam baffles. The study investigated the impact of different values of copper foam pores per inch on the thermohydraulic performance of the system. Aluminum metallic foam baffle was experimentally studied by Hamadouche et al. [25] in a rectangular channel with different baffle height ratios, metal foam grades, and air velocity values. The authors compared the suggested baffles with the regular solid aluminum baffles. An optimum value for the baffle height and metal foam grade was found that achieve the heat transfer rate and pressure drop at the design point. Chen et al. [26] overviewed the use of metal foam baffle in a shell and tube heat exchanger used in waste heat recovery system. The 3D numerical model presented the temperature, velocity, and pressure fields of three types of heat exchangers at various baffle sizes and gas flow rates. The results showed that the suggested baffles enhanced the thermal performance of the system. Graphite foam baffles at various arrangements were experimentally and numerically studied by Leong et al. [27]. The study showed that although the solid baffle achieved the highest heat transfer rate with high-pressure drop, the graphite foam baffles could result in acceptable heat transfer rate at relatively mild pressure drop.

The use of nanofluid to enhance heat transfer has been also examined in recent years. Gholami et al. [28] explored the laminar and forced flow, as well as heat transfer characteristics of oil/multi-walled carbon nanotubes nanofluid within a two-dimensional rectangular microchannel. The investigation focused on the impact of different rib shapes on the behavior and heat transfer of nanofluid flow. The findings revealed that the parabolic rib demonstrates the optimal balance between friction factor augmentation and Nusselt number enhancement. Khodabandeh et al. [29] explored the laminar flow of water nanofluid containing GNP–SDBS nanoparticles in a microchannel with various shapes of ribs. The study highlighted that this microchannel design promotes uniform temperature distribution, and that increasing Reynolds number and solid nanoparticles mass fraction

leads to higher Nusselt numbers and reduced heat resistance on the lower microchannel wall. Varzaneh et al. [30] examined the hydrodynamics and heat transfer characteristics of water/alumina nanofluids in a straight microtube heat sink. The study revealed that an increase in spiral pitch enhances thermal performance by an average of 19.8%. Zhong et al. [31] studied water–Fe3O4 nanofluid within a porous ribbed microchannel heat sink. A direct correlation between porosity percentage, Re and Ha, and the enhancement of the heat transfer coefficient is found in all cases. The study highlighted that the two-phase model yields a higher heat transfer coefficient.

As shown in the previous overview, there are broad studies differ in terms of the heat exchanger application and baffle parameters such as length, shape, inclination, material, and distance. However, the foregoing research that studied the baffles size assumed the same baffle size across the channel although the flow characteristics (velocity, pressure, and temperature) change along the channel. Therefore, this present work suggests using nonidentical baffle lengths across the channel, which, up to authors knowledge, has not been studied in the literature. The objective of changing the length of the baffle is that the fluid characteristics passing the first and second baffles are not identical, so the best baffle length of the first baffle should not be the same best length of the second baffle where the fluid has different characteristics adjacent it. This has been done numerically using ANSYS Fluent 19.2 software. The numerical model has been validated with the well-known experiment and validated model; Demartini et al. [32]. The flow circulation, dynamic pressure, and temperature fields have been presented to overview and discuss the effect of various lengths of the baffles.

Methodology

This work studies the flow inside a two-dimensional channel that has two rectangular baffles (one at the top surface and the other at the bottom surface) as shown in Fig. 1. Assuming an incompressible fluid at steady state in a two-dimensional field, the numerical model can be solved using the continuity equation and conservation of momentum equation. The conservation of mass equation for incompressible flow can be written as follows:

Fig. 1 Two-dimensional channel with two rectangular baffles
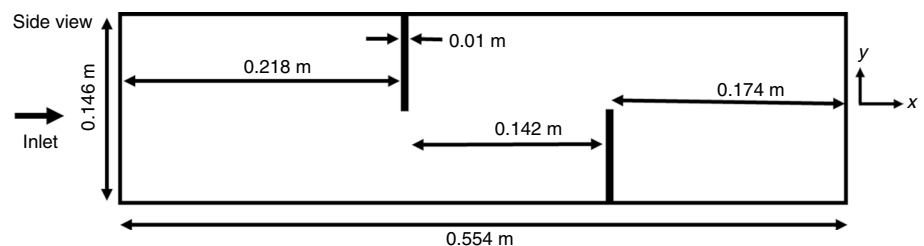
$$\frac{\partial(\rho u)}{\partial x} + \frac{\partial(\rho v)}{\partial y} = 0 \tag{1}$$

where ρ is the density (kg m^{-3}), u is the fluid velocity in x-direction (m s^{-1}), and v is the fluid velocity in y-direction (m s^{-1}). The conservation of momentum in x-direction and y-direction is given by [16]:

$$\frac{\partial\left(\rho u^2\right)}{\partial x} + \frac{\partial(\rho uv)}{\partial y} = -\frac{\partial P}{\partial x} + \frac{\partial}{\partial x}\left[(\mu_1 + \mu_t)\left(\frac{\partial u}{\partial x}\right)\right] + \frac{\partial}{\partial y}\left[(\mu_1 + \mu_t)\left(\frac{\partial u}{\partial y}\right)\right] \tag{2}$$

$$\frac{\partial\left(\rho uv\right)}{\partial x} + \frac{\partial\left(\rho v^2\right)}{\partial y} = -\frac{\partial P}{\partial y} + \frac{\partial}{\partial x}\left[(\mu_1 + \mu_t)\left(\frac{\partial v}{\partial x}\right)\right] + \frac{\partial}{\partial y}\left[(\mu_1 + \mu_t)\left(\frac{\partial v}{\partial y}\right)\right] \tag{3}$$

respectively, where P is the static pressure (Pa), μ_1 is the molecular viscosity (Pas), and μ_t is the turbulent viscosity (Pas). The turbulence is modeled using the k-ε model [15, 16, 33], where the turbulent kinetic energy (k) equation and the turbulent kinetic energy (ε) equation can be given as [16]:

$$\frac{\partial(\rho uk)}{\partial x} + \frac{\partial(\rho vk)}{\partial y} = \frac{\partial}{\partial x}\left[(\mu_1 + \frac{\mu_t}{\sigma_k})\left(\frac{\partial k}{\partial x}\right)\right] + \frac{\partial}{\partial y}\left[(\mu_1 + \frac{\mu_t}{\sigma_k})\left(\frac{\partial k}{\partial y}\right)\right] + G_k + \rho\varepsilon \tag{4}$$

$$\frac{\partial(\rho u\varepsilon)}{\partial x} + \frac{\partial(\rho v\varepsilon)}{\partial y} = \frac{\partial}{\partial x}\left[(\mu_1 + \frac{\mu_t}{\sigma_\varepsilon})\left(\frac{\partial \varepsilon}{\partial x}\right)\right] + \frac{\partial}{\partial y}\left[(\mu_1 + \frac{\mu_t}{\sigma_\varepsilon})\left(\frac{\partial \varepsilon}{\partial y}\right)\right] + G_{1\varepsilon}\frac{\varepsilon}{k} - G_{2\varepsilon}\rho\frac{\varepsilon^2}{k} \tag{5}$$

respectively, where $\mu_t = \rho c_\mu k^2/\varepsilon$; $c_\mu = 0.09$; $\sigma_k = 1.00$; $\varepsilon_k = 1.3$; $G_{1\varepsilon} = 1.44$; and $G_{2\varepsilon} = 1.92$.
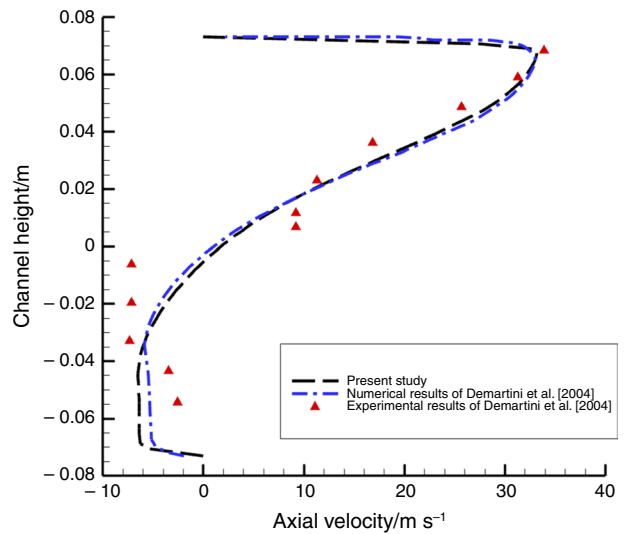
The energy equation:

Fig. 2 Validation with experiment and numerical model of Demartini et al. [32]

$$\rho C_p V \cdot \nabla T = k_f \nabla^2 T \tag{6}$$

where C_p is specific heat (J kg^{-1} K^{-1}), V is the velocity vector (m s^{-1}), k_f is the fluid thermal conductivity (W m^{-1} K^{-1}), and T is temperature (K).

The hydraulic diameter (D_h) and the Reynolds number (Re) are calculated using the following equations, respectively [16]:

$$D_h = \frac{2HW}{(H + W)} \tag{7}$$

$$Re = \frac{\rho U_{in} D_h}{\mu} \tag{8}$$

The local Nusselt number (Nu$_x$), the average Nusselt number (Nu), and the Dittus–Boelter equation for turbulent flow (Nu$_0$) are calculated using the following equations [16]:

$$Nu_x = \frac{h(x)D_h}{k_f} \tag{9}$$

$$Nu = \frac{1}{L}\int Nu_x \partial x \tag{10}$$

$$Nu_0 = 0.023(Re)^{0.8}(Pr)^{0.4} \tag{11}$$

respectively, where L is the heat exchanger length.

The local skin friction coefficient (C_f), average friction coefficient (f), and the Petukhov friction factor correlation (f_0) are calculated using the following formula [16]:

Table 1 Sensitivity of number of elements

# of elements	Average Nu (bottom wall)
4000	283
8000	288
16,000	312
32,000	324
64,000	334
128,000	337

Table 2 Dimensions/in mm of the baffles in the 16 cases

Case #	1	2	3	4	5	6	7	8	9	10	11	12	13	14	15	16
Baffle 1	20	40	60	80	20	40	60	80	20	40	60	80	20	40	60	80
Baffle 2	80	80	80	80	60	60	60	60	40	40	40	40	20	20	20	20
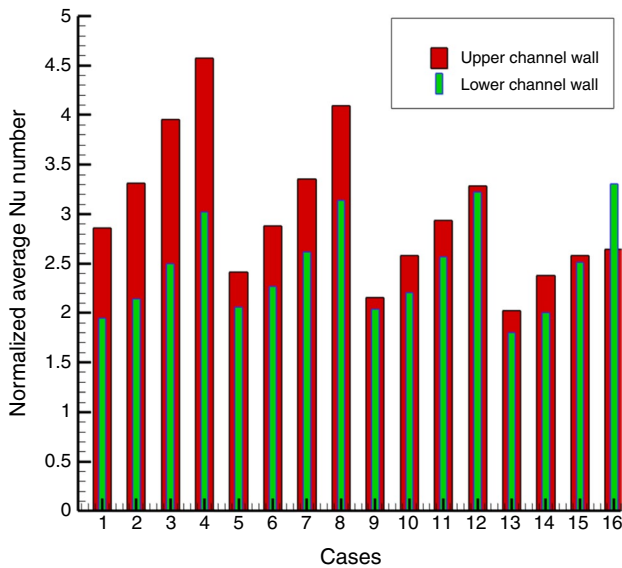
Fig. 3 Average Nusselt number of upper wall and lower wall

Fig. 4 Average friction factor of upper wall and lower wall

$$c_f = \frac{2\tau_w}{\rho U_{in}^2} \quad (12)$$

$$f = \frac{2(\Delta P/L)D_h}{\rho U_{in}^2} \quad (13)$$

$$f_0 = (0.79 \ln Re - 1.64)^{-2} \quad (14)$$

respectively, where τ_w is the wall shear stress, and ΔP is the pressure drop. Finally, the thermal enhancement factor (TEF) is calculated as [16]:

$$TEF = \frac{Nu/Nu_0}{(f/f_0)^{1/3}} \quad (15)$$

The boundary conditions of the model at the inlet (assuming the velocity profile at the channel inlet to be uniform), outlet, walls, and baffles can be shown as the following [32, 34]:

For the inlet section: $u = U_{in} = 4.12 ms^{-1}$; $v = 0$; $k_{in} = 0.005 U_{in}^2$; $\varepsilon_{in} = 0.1 k_{in}^2$, $T_{in} = 300K$.

For the outlet section: $\frac{\partial u}{\partial x} = 0$; $\frac{\partial v}{\partial x} = 0$; $\frac{\partial k}{\partial x} = 0$; $\frac{\partial \varepsilon}{\partial x} = 0$; $P = P_{atm}$.

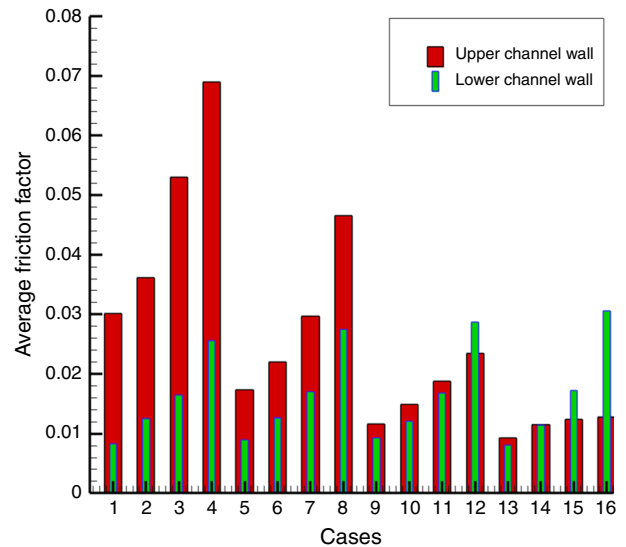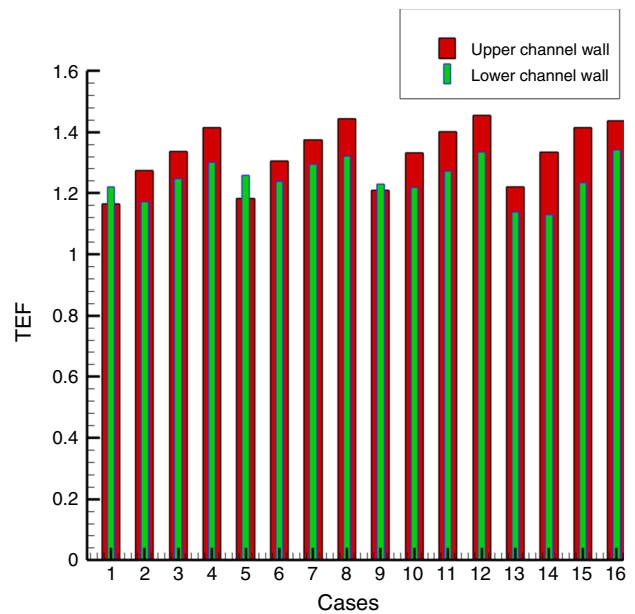At the walls (top and bottom walls): $u = 0$; $v = 0$; $T_{wall} = 375K$.

Fig. 5 Thermal enhancement factor (TEF) of upper wall and lower wall

For the baffles: The baffles are assumed adiabatic, and their material is aluminum. The channel walls and baffles were given non-slip and impermeable boundary conditions.

Several sensitivity tests were conducted to identify the optimal number of elements that would yield accurate results within a shorter computational timeframe. The average Nusselt number on the bottom wall was chosen as the parameter for the sensitivity analysis. Consequently, the examination was executed across six distinct element counts, as outlined in Table 1. The sensitivity outcomes indicate that the Nusselt number's increase stabilizes notably after reaching 64,000 elements. As a result, the utilization of 64,000 elements is deemed suitable for subsequent numerical computations. In terms of solution convergence, the normalized residuals were constrained at 10^{-5} for the continuity and momentum equations, as well as for the variables k and ε, while the energy equation maintained a stricter limit of 10^{-9}. Also, for solution methods, the pressure–velocity coupling scheme is SIMPLE, the second-order method is applied for pressure, and the second-order upwind method is applied across all other problem components, encompassing momentum, k and ε, and energy.

The proposed model has been validated with a well-known experiment and validated model in Demartini et al. [32], where more detail of the experiment and the model can be found. The comparison between the present model and the experiment is shown in Fig. 2 for the axial velocity at x = 0.525 m and Re = 87,300, which shows a good agreement between the results.

Results and discussion

There are many parameters in the heat exchanger that can be studied including Nusselt number, friction factor, temperature, pressure drop, velocity, etc. In addition, in terms
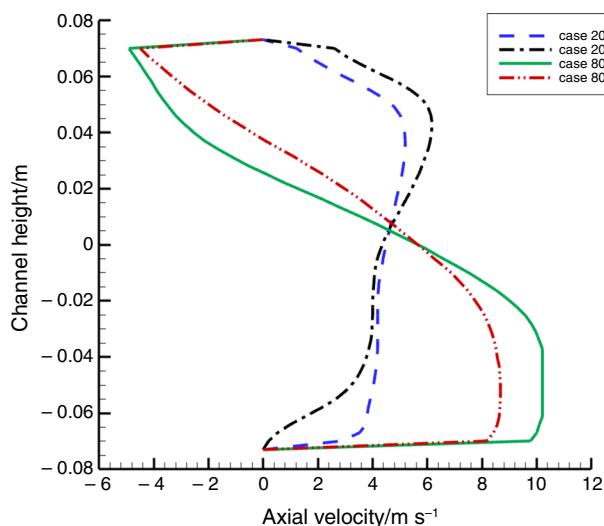
of studying the effect of nonidentical baffle lengths, there are combinations of the baffle length. Therefore, this section will be divided into studying 16 cases of different baffle sizes, then four specific cases are chosen from those 16 cases for further analysis. The detail of those cases is shown in Table 2. Reynolds number in all cases is constant and equals to 47,000.

Examining the average Nusselt number of upper and lower wall of the 16 cases, which is shown in Fig. 3, presents that the difference between the average Nusselt number of the upper and lower walls is greater when the second baffle is long. Case number 16 is the only case where the average Nusselt number of the upper wall is less than the
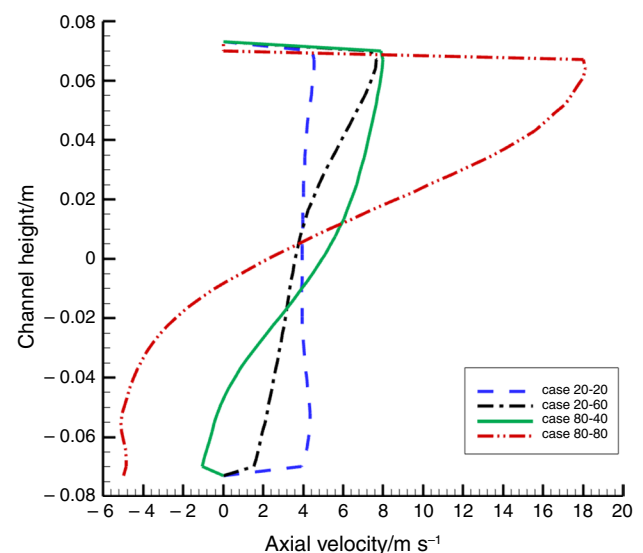

Fig. 7 Axial velocity before the second baffle at x = 0.355 m

Fig. 6 Axial velocity after the first baffle at x = 0.315 m

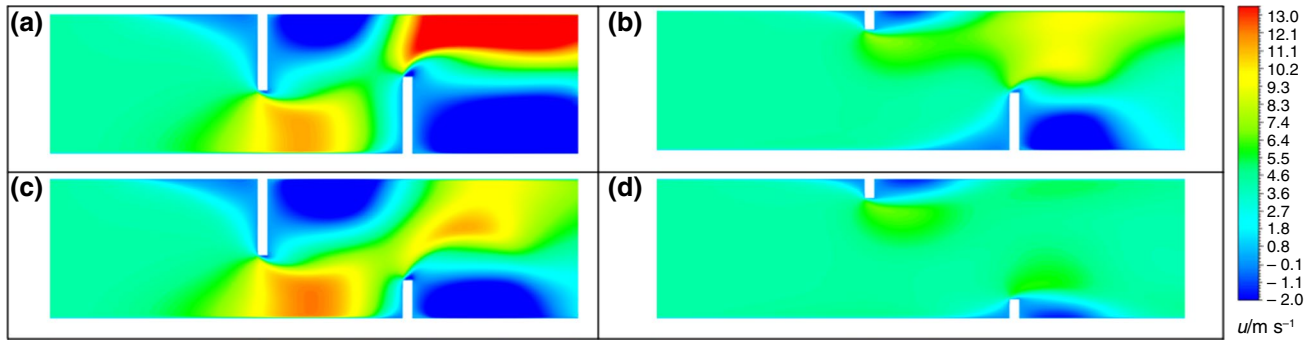**Fig. 8** Axial velocity before the channel end at x = 0.525 m

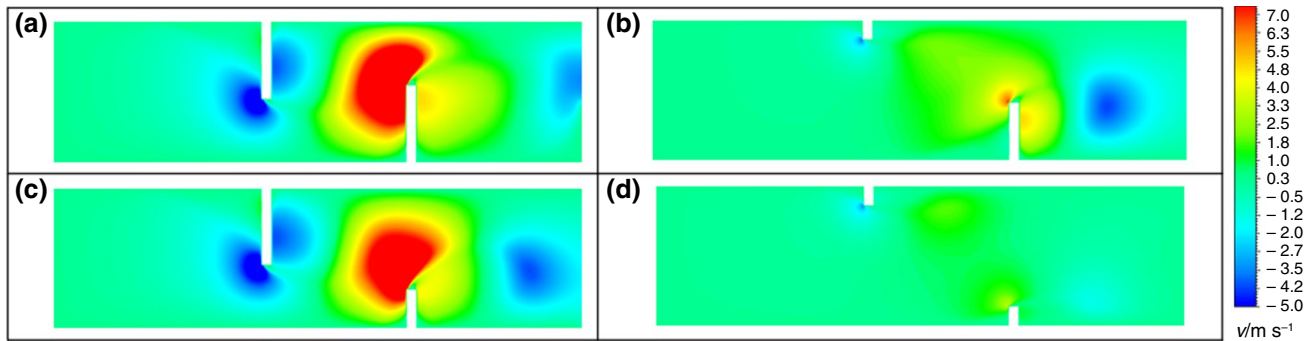**Fig. 9** X-velocity of **a** case 4, **b** case 5, **c** case 12, and **d** case 13

Fig. 10 Y-velocity of **a** case 4, **b** case 5, **c** case 12, and **d** case 13
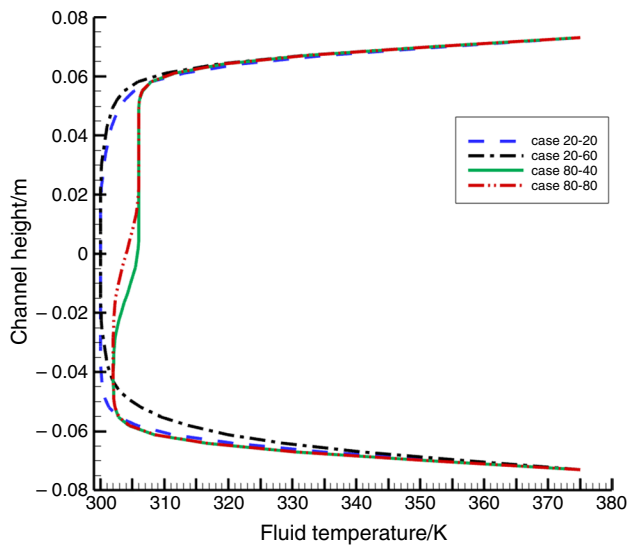

Fig. 11 Fluid temperature after the first baffle at x = 0.315 m
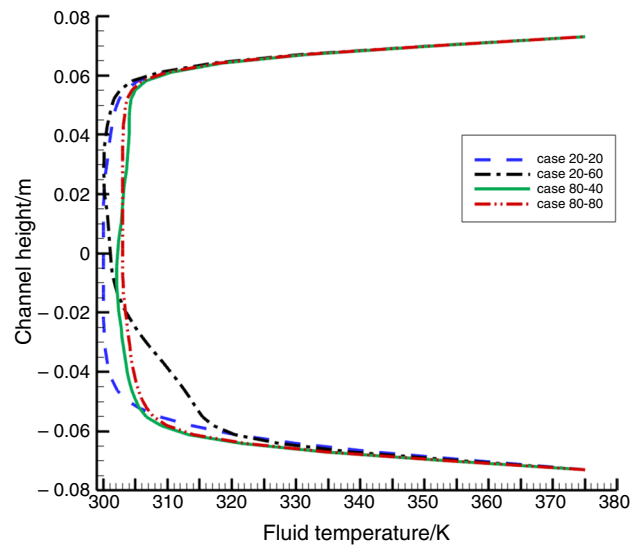

Fig. 12 Fluid temperature before the second baffle at x = 0.355 m

average Nusselt number of the lower wall. The average Nusselt number of the upper wall increases almost linearly with the increase length of the first baffle when the second baffle length is constant. The average Nusselt number of the upper wall also increases almost linearly with the increase length

of the second baffle when the first baffle length is constant. However, for the lower wall, the average Nusselt number of the lower wall only increases with the increase in the first baffle length while the second baffle length is constant, but it almost does not change when the second baffle length
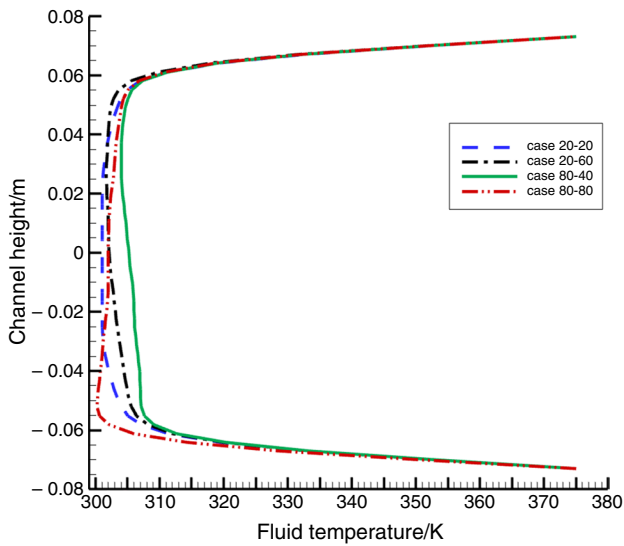
Fig. 13 Fluid temperature before the channel end at x = 0.525 m

increases while the first baffle length is constant. In short, the average Nusselt number of the upper wall is sensitive to the length of both baffles, while the average Nusselt number of the lower wall is only sensitive to the length of the first baffle. Another interesting point here is that the four cases where the baffles have the same length (cases number 4, 7, 10, and 13) do not always have the highest value of Nusselt number. The highest value of Nusselt number in the upper wall is achieved when both baffles are the longest (cases 3, 4, and 8), and the highest value of Nusselt number in the lower wall is achieved when the first baffle is the longest (cases 4, 8, 12, and 16). From this result, the assumption that the baffles inside the channel should not be identical is valid, at least for the effect on the Nusselt number.

When examining the average friction factor for the two walls in the 16 cases as shown in Fig. 4, the same pattern from the average Nusselt number is shown. In other words, the average friction factor of the upper wall increases with
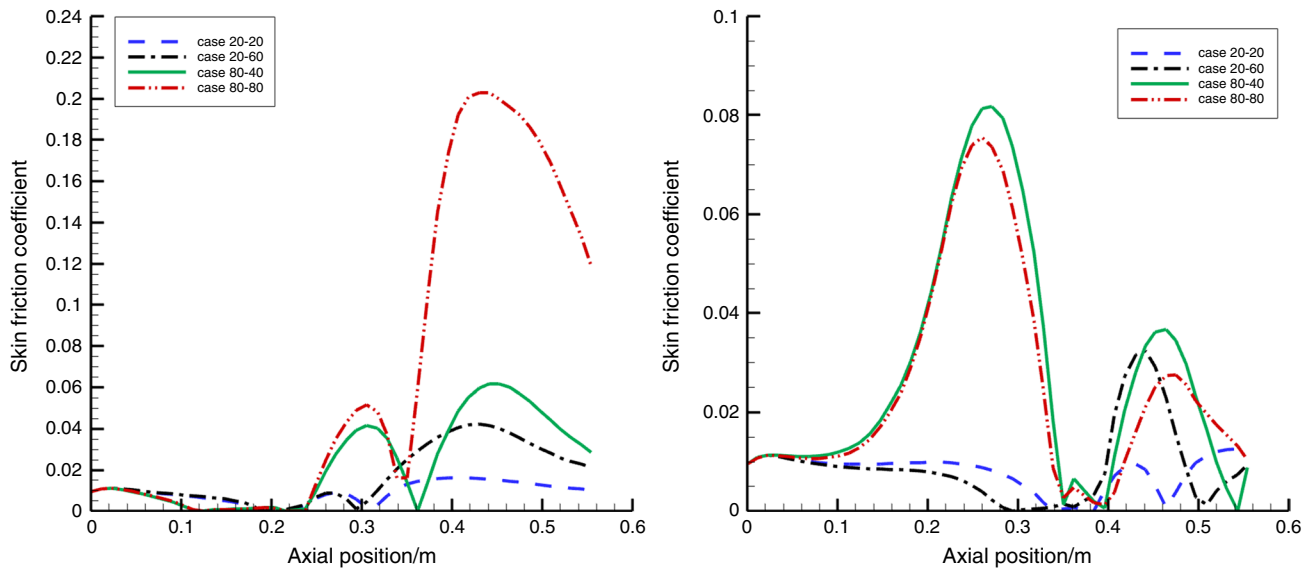

Fig. 14 Friction factor along the upper wall (left) and lower wall (right)
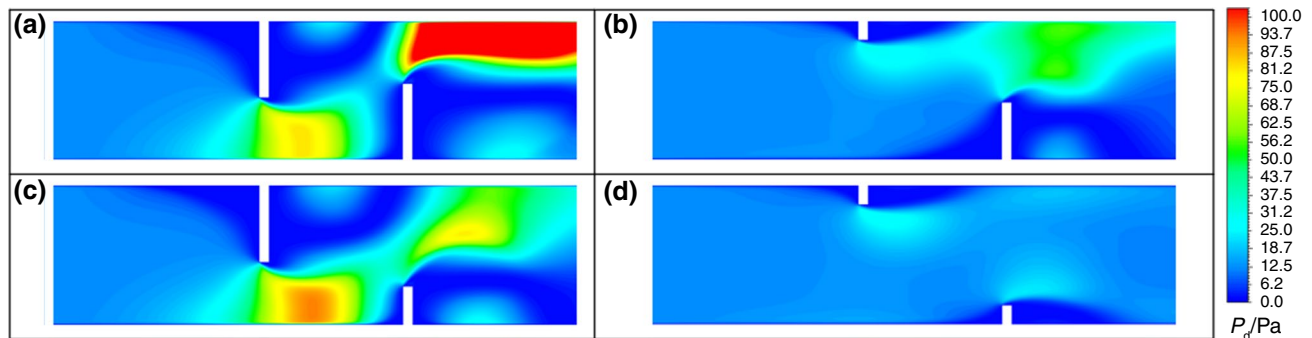

Fig. 15 Dynamic pressure of **a** case 4, **b** case 5, **c** case 12, and **d** case 13
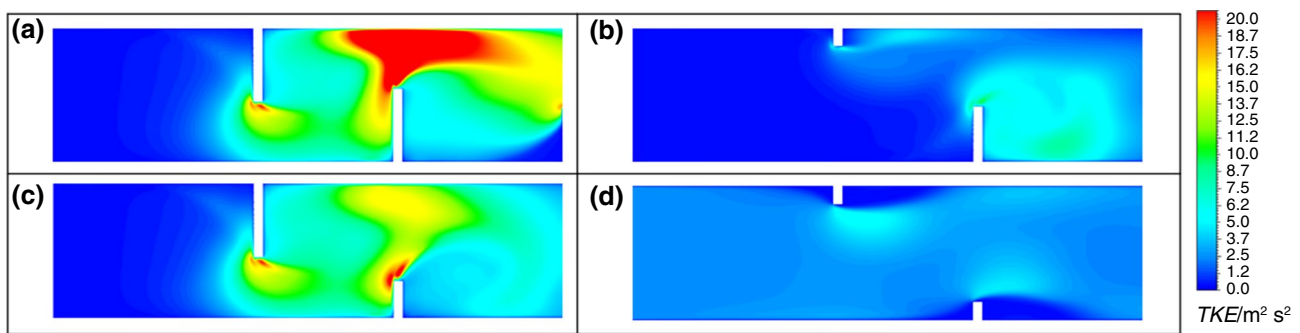
Fig. 16 Turbulence kinetic energy of **a** case 4, **b** case 5, **c** case 12, and **d** case 13

the increase length of a baffle when the other baffle length is constant. And the average friction factor of the lower wall only increases with the increase in the first baffle length while the second baffle length is constant, but it almost does not change when the second baffle length increases while the first baffle length is constant. Therefore, the identical baffles in length do not always achieve the lowest friction factor.

To choose the optimum case that achieves that best result of the heat exchanger, thermal enhancement factor, or TEF, is used here since it combines the result of both Nusselt number and friction factor. Figure 5 depicts that the best cases are when the first baffle is the longest (cases number 12, 16, 8, and 4). Overall, the TEF increases with the increase in the first baffle length regardless of the length of the second baffle. The best case among the 16 cases is case number 12, where the second baffle is half the length of the first baffle (40 and 80 mm, respectively). This case is 3% better than the case number 4, where both baffle lengths are equal to 80 mm. Hence, the assumption that the baffles inside the channel should not be identical in length is valid.

To further analyze the results, four cases have been chosen: the best case (case number 12), the worst case (case number 13), and two random cases (cases number 4 and 5). Figures 6–8 present the axial velocity for these four cases at three locations: after the first baffle at x = 0.315 m, before the second baffle at x = 0.355 m, and at the end of the channel at x = 0.525 m, respectively.

For case number 13 (the worst case), the axial velocity in the three locations is barely affected by the baffles because both baffles are relatively short, so the axial velocity did not augment compared to the other cases. This is shown clearly in Figs. 9d and 10d where the x- and y-velocity slightly change. For case number 12 (the best case), the axial velocity reaches high value (over 10 m s^{-1}) just after the first baffle, before it drops to around 8 m s^{-1} at the end of the channel because the second baffle is shorter than the first channel. However, when the second channel length stays the same (case number 4), the axial speed further increases to reach 18 m s^{-1} at the end of the channel. This can be visualized

in Fig. 9a and c where less fluid circulation (negative axial velocity) is shown after the second baffle in case number 12. This difference is one that emphasizes the nonidentical baffle length as proven earlier when the TEF was compared. For case number 5, the axial velocity reaches around 7.8 m s^{-1} at maximum at the end of the channel. The first baffle is relatively short to affect the behavior of the fluid, and Figs. 9b and 10b show that most of the changes in x- and y-velocity occurs around the second baffle.

Figures 11–13 present the temperature for the four cases at the same three locations. The highest increase in temperature of the fluid at the first location (after the first baffle) occurs for the cases with first baffle is 80 mm (cases number 4 and 12). This is because the long first baffle creates more turbulence and recirculation fluid as shown in Figs. 9a–d and 10a–d. The case number 5 has higher temperature at the bottom surface after the first baffle because the second baffle creates higher negative axial velocity between the two baffles. In general, the case number 12 (the best case) has the highest increase in temperature of the fluid at the three locations.

The friction factor for the four cases along the upper and lower walls is shown in Fig. 14. The case number 13 (the worst case) has the lowest friction factor at the upper and lower walls. The relatively long first baffle for the cases number 4 and 12 generates higher friction factor at the upper and lower walls around the first baffle. Around the second baffle, the friction factor extremely increases at the upper wall in case number 4 because the second baffle length stays the same. On the other hand, the decrease in the second baffle length in case number 12 insignificantly increases the friction factor at the upper wall. In general, the cases with longer baffles have higher friction factors as expected.

The dynamic pressure inside the channel is shown in Fig. 15 for the four cases. The first baffle barely changes the dynamic pressure in cases number 5 and 13 because its length is relatively small. Only when the second baffle length is increased in case number 5, the dynamic pressure rises after the second baffle at the top part of the channel.

The dynamic pressure in significantly increases from the first baffle at cases number 4 and 12, where the baffle lengths are relatively high. Around the second baffle, enormous increase in the dynamic pressure around the upper wall in case number 4 because the second baffle length stays the same.

The same behavior can be seen for the turbulence kinetic energy (TKE) in Fig. 16. While small TKE is small for the cases number 5 and 13, it is significant in cases number 4 and 12 due to the longer baffles. When the second baffle stays the same in case number 4, the TKE extremely increases around the second baffle compared to case number 12, where the second baffle length is shorter than the first baffle.

Conclusions

While the foregoing research that studied the baffles size assumed the same baffle size across the channel although the flow characteristics (velocity, pressure, and temperature) change along the channel, this present work suggested using nonidentical baffle lengths across the channel. The best baffle length of the first baffle may not be the same best length of the second baffle where the fluid has different characteristics adjacent it. This has been done numerically using a two-dimensional channel in ANSYS Fluent software. After studying 16 cases of different baffle sizes with Reynolds number in all cases is constant and equals to 47,000, the main outcomes are:

1. The baffles that have the same length do not always have the highest Nusselt number or the lowest friction factor.
2. The average Nusselt number of the upper wall is sensitive to the length of both baffles, while the average Nusselt number of the lower wall is only sensitive to the length of the first baffle.
3. The best case in the thermal enhancement factor is case number 12, where the second baffle is half the length of the first baffle, and the first baffle length is almost equal to half of the channel height.
4. At the upper wall around the second baffle, the friction factor extremely increases when the second baffle length stays the same; however, the decrease in the second baffle length insignificantly increases the friction factor and the axial velocity.

From this result, the assumption that the baffles inside the channel should not be identical in length is valid. Further studies are needed to consider other factors such as Reynolds number, the dimensions of the channel, and baffle's shape, direction, and material.

References

1. Marzouk SA, Abou Al-Sood MM, El-Said EMS, El-Fakharany MK, Younes MM. Study of heat transfer and pressure drop for novel configurations of helical tube heat exchanger: a numerical and experimental approach. J Therm Anal Calorim. 2023;148:6267–82. https://doi.org/10.1007/s10973-023-12067-7.
2. Andrzejczyk R, Muszynski T. Thermodynamic and geometrical characteristics of mixed convection heat transfer in the shell and coil tube heat exchanger with baffles. Appl Therm Eng. 2017;121:115–25. https://doi.org/10.1016/j.applthermaleng.2017.04.053.
3. Miansari M, Jafarzadeh A, Arasteh H, Toghraie D. Thermal performance of a helical shell and tube heat exchanger without fin, with circular fins, and with V-shaped circular fins applying on the coil. J Therm Anal Calorim. 2021;143:4273–85. https://doi.org/10.1007/s10973-020-09395-3.
4. Sabau AS, Nejad AH, Klett JW, Bejan A, Ekici K. Novel evaporator architecture with entrance-length crossflow-paths for supercritical organic Rankine cycles. Int J Heat Mass Transf. 2018;119:208–22. https://doi.org/10.1016/j.ijheatmasstransfer.2017.11.042.
5. Nejad AH, Ekici K, Sabau AS, Bejan A, Arimilli RV. Counter cross-flow evaporator geometries for supercritical organic Rankine cycles. Int J Heat Mass Transf. 2019;135:425–35. https://doi.org/10.1016/j.ijheatmasstransfer.2019.01.134.
6. Afzal A, Islam MdT, Kaladgi AR, Manokar AM, Samuel OD, Mujtaba MA, et al. Experimental investigation on the thermal performance of inserted helical tube three-fluid heat exchanger using graphene/water nanofluid. J Therm Anal Calorim. 2022;147:5087–100. https://doi.org/10.1007/s10973-021-10869-1.
7. ShahsavarGoldanlou A, Sepehrirad M, Papi M, Hussein AK, Afrand M, Rostami S. Heat transfer of hybrid nanofluid in a shell and tube heat exchanger equipped with blade-shape turbulators. J Therm Anal Calorim. 2021;143:1689–700. https://doi.org/10.1007/s10973-020-09893-4.
8. Marzouk SA, Aljabr A, Almehmadi FA, Alqaed S, Sharaf MA. Numerical study of heat transfer, exergy efficiency, and friction factor with nanofluids in a plate heat exchanger. J Therm Anal Calorim. 2023. https://doi.org/10.1007/s10973-023-12441-5.
9. Marzouk SA, Abou Al-Sood MM, El-Said EMS, Younes MM, El-Fakharany MK. A comprehensive review of methods of heat transfer enhancement in shell and tube heat exchangers. J Therm Anal Calorim. 2023;148:7539–78. https://doi.org/10.1007/s10973-023-12265-3.
10. Brahimi A, Rebhi R, Alliche M. Numerical study of the effects of roughness coupled with inclination on a turbulent flow around an obstacle. Processes. 2023;11:1979. https://doi.org/10.3390/pr11071979.
11. Cao X, Du T, Liu Z, Zhai H, Duan Z. Experimental and numerical investigation on heat transfer and fluid flow performance of

sextant helical baffle heat exchangers. Int J Heat Mass Transf. 2019;142:118437.

12. Skullong S, Thianpong C, Jayranaiwachira N, Promvonge P. Experimental and numerical heat transfer investigation in turbulent square-duct flow through oblique horseshoe baffles. Chem Eng Process. 2016;99:58–71. https://doi.org/10.1016/j.cep.2015.11.008.

13. Promvonge P, Skullong S. Thermal-hydraulic performance enhancement of solar receiver channel by flapped V-baffles. Chem Eng Res Des. 2022;182:87–97. https://doi.org/10.1016/j.cherd.2022.03.051.

14. Saha S. Numerical study of air-flow phenomena through a baffled rectangular micro-channel. J Model Optim. 2021;13:51–7. https://doi.org/10.32732/jmo.2021.13.2.51.

15. Menni Y, Ghazvini M, Ameur H, Ahmadi MH, Sharifpur M, Sadeghzadeh M. Numerical calculations of the thermal-aerodynamic characteristics in a solar duct with multiple V-baffles. Eng Appl Comput Fluid Mech. 2020;14:1173–97. https://doi.org/10.1080/19942060.2020.1815586.

16. Medjahed DM, Ameur H, Rebhi R, Inc M, Ahmad H, Menni Y, et al. Details on the hydrothermal characteristics within a solar-channel heat-exchanger provided with staggered t-shaped baffles. Energies (Basel). 2021. https://doi.org/10.3390/en14206698.

17. Mohammadi K, Sabzpooshani M. Comprehensive performance evaluation and parametric studies of single pass solar air heater with fins and baffles attached over the absorber plate. Energy. 2013;57:741–50. https://doi.org/10.1016/j.energy.2013.05.016.

18. Kumar R, Kumar A, Goel V. A parametric analysis of rectangular rib roughened triangular duct solar air heater using computational fluid dynamics. Sol Energy. 2017;157:1095–107. https://doi.org/10.1016/j.solener.2017.08.071.

19. El-Said EMS, Abou Al-Sood MM. Shell and tube heat exchanger with new segmental baffles configurations: a comparative experimental investigation. Appl Therm Eng. 2019;150:803–10. https://doi.org/10.1016/j.applthermaleng.2019.01.039.

20. Marzouk SA, Al-Sood MMA, El-Fakharany MK, El-Said EMS. A comparative numerical study of shell and multi-tube heat exchanger performance with different baffles configurations. Int J Therm Sci. 2022;179:107655. https://doi.org/10.1016/j.ijthermalsci.2022.107655.

21. El HabetAhmed MASA, Saleh MA. The effect of using staggered and partially tilted perforated baffles on heat transfer and flow characteristics in a rectangular channel. Int J Therm Sci. 2022;174:107422. https://doi.org/10.1016/j.ijthermalsci.2021.107422.

22. Rebhi R, Ahmad H, Zhao Y-H, Menni Y, Lorenzini G. Numerical assessment of an air-heat exchanger channel with staggered attached rectangular baffles and in-line detached square fins. Therm Sci. 2023;27:343–51. https://doi.org/10.2298/TSCI23S1343R.

23. Kitayama S, Miyamoto K, Izutsu R, Tabuchi S, Yamada S. Numerical optimization of baffle configuration in header of heat exchanger using sequential approximate optimization. Simul Model Pract Theory. 2022;115:102429. https://doi.org/10.1016/j.simpat.2021.102429.

24. Fadhala K, Fayyadh E, Mohammed A. Experimental investigation on the thermal-hydraulic performance of channel with gradient metal foam baffles. FME Transactions. 2023;51:14–22. https://doi.org/10.5937/fme2301014F.

25. Hamadouche A, Azzi A, Abboudi S, Nebbali R. Enhancement of heat exchanger thermal hydraulic performance using aluminum foam. Exp Therm Fluid Sci. 2018;92:1–12. https://doi.org/10.1016/j.expthermflusci.2017.10.035.

26. Chen T, Shu G, Tian H, Zhao T, Zhang H, Zhang Z. Performance evaluation of metal-foam baffle exhaust heat exchanger for waste heat recovery. Appl Energy. 2020;266:114875. https://doi.org/10.1016/j.apenergy.2020.114875.

27. Leong KC, Li HY, Jin LW, Chai JC. Numerical and experimental study of forced convection in graphite foams of different configurations. Appl Therm Eng. 2010;30:520–32. https://doi.org/10.1016/j.applthermaleng.2009.10.014.

28. Gholami MR, Akbari OA, Marzban A, Toghraie D, Shabani GAS, Zarringhalam M. The effect of rib shape on the behavior of laminar flow of oil/MWCNT nanofluid in a rectangular microchannel. J Therm Anal Calorim. 2018;134:1611–28. https://doi.org/10.1007/s10973-017-6902-3.

29. Khodabandeh E, Rozati SA, Joshaghani M, Akbari OA, Akbari S, Toghraie D. Thermal performance improvement in water nanofluid/GNP–SDBS in novel design of double-layer microchannel heat sink with sinusoidal cavities and rectangular ribs. J Therm Anal Calorim. 2019;136:1333–45. https://doi.org/10.1007/s10973-018-7826-2.

30. Varzaneh AA, Toghraie D, Karimipour A. Comprehensive simulation of nanofluid flow and heat transfer in straight ribbed microtube using single-phase and two-phase models for choosing the best conditions. J Therm Anal Calorim. 2020;139:701–20. https://doi.org/10.1007/s10973-019-08381-8.

31. Zhong J-F, Sedeh SN, Lv Y-P, Arzani B, Toghraie D. Investigation of Ferro-nanofluid flow within a porous ribbed microchannel heat sink using single-phase and two-phase approaches in the presence of constant magnetic field. Powder Technol. 2021;387:251–60. https://doi.org/10.1016/j.powtec.2021.04.033.

32. Demartini LC, Vielmo HA, Möller SV. Numeric and experimental analysis of the turbulent flow through a channel with baffle plates. J Braz Soc Mech Sci Eng. 2004;26:153–9. https://doi.org/10.1590/S1678-58782004000200006.

33. Launder BE, Spalding DB. The numerical computation of turbulent flows. Comput Methods Appl Mech Eng. 1974;3:269–89. https://doi.org/10.1016/0045-7825(74)90029-2.

34. Nasiruddin, Siddiqui MHK. Heat transfer augmentation in a heat exchanger tube using a baffle. Int J Heat Fluid Flow. 2007;28:318–28. https://doi.org/10.1016/j.ijheatfluidflow.2006.03.020.